Fast Track Article
**This paper is dedicated to
the memory of Werner Schreyer**

Boromullite, $Al_9BSi_2O_{19}$, a new mineral from granulite-facies metapelites, Mount Stafford, central Australia: a natural analogue of a synthetic "boron-mullite"

Ian S. Buick[1], Edward S. Grew[2,*], Thomas Armbruster[3], Olaf Medenbach[4], Martin G. Yates[2], Gray E. Bebout[5] and Geoffrey L. Clarke[6]

[1] Research School of Earth Sciences, The Australian National University, Canberra, ACT 0200, Australia
[2] Department of Earth Sciences, University of Maine, 5790 Bryand Research Center, Orono, Maine 04469-5790, USA
*Corresponding author, e-mail: esgrew@maine.edu
[3] Institut für Geologie, Gruppe Mineralogie-Kristallographie, Universität Bern, Freiestrasse 3, 3012 Bern, Switzerland
[4] Institut für Geowissenschaften/Mineralogie, Ruhr-Universität Bochum, 44780 Bochum, Germany
[5] Department of Earth & Environmental Sciences, Lehigh University, 31 Williams Drive, Bethelem, PA 18015, USA
[6] School of Geosciences, University of Sydney, NSW 2006, Australia

Abstract: Boromullite is a new mineral corresponding to a 1:1 polysome composed of Al_5BO_9 and Al_2SiO_5 modules. Electron-microprobe analysis of the holotype prism is SiO_2 19.01(1.12), TiO_2 0.01(0.02), B_2O_3 6.52(0.75), Al_2O_3 74.10(0.95), MgO 0.07(0.03), CaO 0.00(0.02), MnO 0.01(0.04), FeO 0.40(0.08), Sum 100.12 wt.%, which gives $Mg_{0.01}Fe_{0.03}Al_{8.88}Si_{1.93}B_{1.14}O_{18.94}$ (normalised to 12 cations), ideally $Al_9BSi_2O_{19}$. Overall, in the type specimen, it ranges in composition from $Mg_{0.01}Fe_{0.03}Al_{8.72}Si_{2.44}B_{0.80}O_{19.20}$ to $Mg_{0.01}Fe_{0.03}Al_{9.22}Si_{1.38}B_{1.35}O_{18.67}$. Single-crystal X-ray diffraction gives orthorhombic symmetry, $Cmc2_1$, a 5.7168(19) Å, b 15.023(5) Å, c 7.675(3) Å, V 659.2(7) Å^3, calculated density 3.081 g/cm^3, $Z = 2$. The refined structure model indicates two superimposed modules present in equal proportions in the holotype prism. Module 1 has the topology and stoichiometry of sillimanite and carries all the Si, whereas module 2 is a type of mullite defect structure in which Si is replaced by B in triangular coordination and by Al in tetrahedral coordination, *i.e.*, Al_5BO_9. The strongest lines in the powder pattern [d in Å, ($I_{meas.}$), (hkl)] are 5.37(50) (021), 3.38(100) (022, 041), 2.67 (60) (042), 2.51(60) (221, 023), 2.19(80) (222), 2.11(50) (043), 1.512(80) (263). Boromullite is colourless and transparent, biaxial (+), n_x 1.627(1), n_y 1.634(1), n_z 1.649(1) (589 nm). $2V_z$ (meas) = 57(2)°, $2V_z$ (calc) = 69(12)°. In the type specimen boromullite tends to form prisms or bundles of prisms up to 0.4 mm long, typically as fringes or overgrowths on aggregates of sillimanite or as narrow overgrowths around embayed werdingite prisms. In other samples boromullite and sillimanite are intergrown on a fine scale (from < 1 μm to > 10 μm). Sekaninaite-cordierite, potassium feldspar, biotite, werdingite and its Fe-dominant analogue, hercynite, and ilmenite are other commonly associated minerals, whereas ominelite-grandidierite, plagioclase, andalusite, and tourmaline are much subordinate. The most widespread accessories are monazite-(Ce), an apatite-group mineral and zircon. Boromullite formed during anatexis of B-rich pelitic rocks under granulite facies conditions (810 °C ≈ T ≥ 775–785 °C, P = 3.3–4 kbar), possibly due to a shift in bulk composition to lower SiO_2 and B_2O_3 contents associated with melt extraction. The assemblage boromullite + cordierite + sillimanite lies at lower SiO_2 and B_2O_3 contents than the assemblage werdingite + cordierite + sillimanite and thus a decrease in SiO_2 and B_2O_3 leads to the replacement of werdingite by boromullite, consistent with textural relations.

Key-words: boron, new mineral, Australia, electron microprobe, crystal structure, granulite facies, anatexis, boromullite.

Introduction

Werner Schreyer and his colleague Günter Werding gave the name "B-mullite" to a phase having an X-ray pattern similar to that Scholze (1956) reported for the mullite-like Al-borate "$9Al_2O_3 \cdot 2B_2O_3$" (Werding & Schreyer, 1984). Werding & Schreyer (1996) revised this term to "boron-mullite" and applied it to ternary mullite-like phases synthesised in the B_2O_3-Al_2O_3-SiO_2-H_2O (BASH) system. They inferred a compositional range for "boron-mullites"

extending over the quadrilateral bounded by vertices of 2:1- and 3:2-mullite, Al_5BO_9, and $AlBO_3$ (Fig. 1). Some of these "boron-mullites" were synthesised in the presence of BAS melts at conditions not attained in geological systems, *viz.* 1200–1600 °C at 1 bar (Dietzel & Scholze, 1955; Gelsdorf *et al.*, 1958), whereas others were produced from gels over a wide range of conditions in part overlapping with crustal conditions, *viz.* 500–1300 °C, 1 bar–8 kbar (Letort, 1952; Werding & Schreyer, 1984, 1992, 1996; Griesser *et al.*, 2008). Although several were
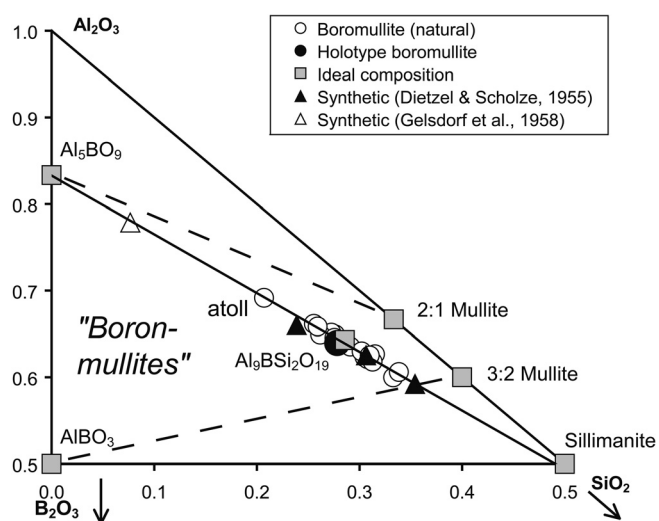
Fig. 1. Compositional plot (mole fraction) of boromullite in sample 2006-MST22 (circles), "boron-mullite" synthesised in the presence of melt (triangles) and compositional range for "boron-mullites" inferred by Werding & Schreyer (1996), *i.e.*, the quadrilateral (dashed lines) defined by vertices at 2:1- and 3:2-mullite, Al_5BO_9, and $AlBO_3$. Least squares fit for sample 2006-MST22 gives $Al_2O_3 = -0.6784*SiO_2 + 0.8327$, $R^2 = 0.9702$. Following Grew *et al.* (2008), we have included in the averages only analyses totaling 98–102 wt.% and containing less than 0.5 wt.% MgO and 1.2 wt.% FeO. Atoll refers to texture illustrated in Fig. 7b, d.

Table 1. X-ray powder-diffraction data for boromullite.

I_{meas}	d_{meas}	d_{calc}	I_{calc}	$h\,k\,l$
50	5.37	5.368	88	0 2 1
–	–	4.385	23	1 1 1*
–	–	3.767	10	1 3 0*
100	3.38	3.417	57	0 2 2
		3.374	100	0 4 1
10	2.84	2.859	17	2 0 0
60	2.67	2.684	51	0 4 2
60	2.51	2.523	53	2 2 1
–	–	2.422	13	0 2 3
20	2.26	2.275	20	2 4 0
80	2.19	2.193	65	2 2 2
50	2.11	2.114	26	0 4 3
5	1.828	1.829	12	2 6 1
30	1.682	1.691	12	2 6 2
		1.687	15	0 8 2
20	1.588	1.593	18	2 0 4
5	1.562	1.570	7	2 8 0
80	1.512	1.517	49	2 6 3
5	1.447	1.453	10	2 8 2
20	1.420	1.429	22	4 0 0
10	1.329	1.331	19	2 2 5
5	1.305	1.319	4	4 2 2
		1.316	7	4 4 1
		1.310	5	2 10 1
10	1.268	1.272	11	2 4 5
		1.262	7	4 4 2
10	1.251	1.257	14	2 10 2

Notes: *Superstructure reflection. Calculated data from LAZY PULVERIX (Yvon *et al.*, 1977) based on single-crystal refinement: *a* 5.7168(19) Å, *b* 15.023(5) Å, *c* 7.675(3) Å.

analysed chemically and the general relationship with mullite established with X-ray powder diffraction, none of the ternary "boron-mullites" in the B_2O_3-Al_2O_3-SiO_2 system has been studied with single-crystal or other methods that would allow detailed crystallographic comparison with related structures.

Grew *et al.* (2008) reported in three samples of granulite-facies metapelite from Mount Stafford, central Australia, what electron microprobe analyses suggested could be a "natural 'boron-mullite'". However, the mineral was too fine-grained to obtain X-ray diffraction or optical data, and thus Grew *et al.* (2008) were not able to fully characterise the mineral. Subsequently, a fourth sample, which was collected in 2006, turned out to contain coarser-grained prisms of the mineral, a few of which were suitable for crystallographic and optical study, and only then were we able to successfully obtain the information required to describe the natural "boron-mullite" as the new mineral boromullite. The type locality (2006-MST22) is situated about 170 km northwest of Alice Springs, central Australia. Its grid reference on the 1:100 000 map "Geology of the Reynolds Range Region, Northern Territory (1981)" and the Australian Map Grid, Zone 53 is 02 59869 (easting), 75 62372 (northing), or about 22° 01′ S, 132° 40′ E. The mineral and name were approved by the Commission on New Minerals, Nomenclature and Classification, International Mineralogical Association (2007-021). Boromullite is named for boron being an essential constituent and for its relationship to mullite. Type material is deposited in the South Australian Museum, Science Centre, Morgan Thomas Lane (off Kintore Avenue), Adelaide, South Australia 5000, Australia; registration numbers SAM G31520 (holotype) and SAM G31521 (2 pieces of cotype); these are fragments of sample 2006-MST22.

Analytical methods

The optical properties of boromullite (section a/area 2/grain 2) were measured at the Ruhr-Universität Bochum by routine immersion procedure using a microrefractometre spindle-stage (Medenbach, 1985).

X-ray powder-diffraction data were obtained from boromullite (section a/area 4/grain 2) with a 57.3 mm diameter Gandolfi camera and Cu$K\alpha$ radiation at the Ruhr-Universität Bochum (Table 1).

Cell dimensions (Table 2) of boromullite (section a/area 2/grain 2) were refined from reflections at scattering angles $13 < \theta < 20°$ obtained with graphite-monochromated Mo$K\alpha$ radiation on an ENRAF NONIUS CAD4 diffractometer equipped with a point detector at the Universität Bern. CAD4 instrumentation gives higher accuracy albeit similar precision as the CCD instrument.

For the structure analysis, the same grain of boromullite (section a/area 2/grain 2) was mounted on a Bruker PLATFORM three-circle goniometer equipped with a 1 K SMART CCD detector and a crystal-to-detector distance of 5.4 cm (Table 2). The studied disc-like crystal

Table 2. Parameters for X-ray data collection and crystal-structure refinement of boromullite.

Diffractometer	Siemens Smart CCD 1K
X-ray radiation	$MoK\alpha$ (0.71073 Å)
X-ray power	50 kV, 40 mA
Temperature	293 K
Crystal size (mm)	$0.10 \times 0.10 \times 0.03$
Detector to sample distance	5.4 cm
Rotation axis	ω
Rotation width	0.5°
Total number of frames	980
Frame size	512×512 pixels
Time per frame	30 sec
Space group	$Cmc2_1$ (Nr. 36)
Cell dimensions (Å)	a 5.7168(19)
	b 15.023(5)
	c 7.675(3)
Cell volume (Å^3)	659.2(7)
Z	2
Collection mode	automated hemisphere
Reflections collected	2313
Max. 2θ	55.3
Index range	$-7 \leq h \leq 7$
	$-15 \leq k \leq 19$
	$-9 \leq l \leq 9$
Unique reflections	771
Reflections $> 2\sigma(I)$	527
R_{int}	0.064
R_σ	0.081
Number of least squares parameters	86
GooF	0.984
$R1$, $I > 2\sigma(I)$	0.0484
$R1$, all data	0.0858
w$R2$ (on F^2)	0.0953
$\Delta\rho_{min}$ ($-e$.Å^{-3})	0.4 close to Al1
$\Delta\rho_{max}$ (e.Å^{-3})	0.7 close to O7

Note: Definitions of R_{int}, R_σ, $R1$, and w$R2$ are given in Bruker (1997).

Table 3. Atomic coordinates and isotropic displacement parameters, with standard deviation in parentheses, for boromullite.

site	occupancy	x.	y.	z.	U_{iso}
Al1	Al	0.2544(3)	0.1212(2)	0.6536(4)	0.0118(4)
Al2	0.5 Al + 0.5 Si	0.0000	0.2980(2)	0.4943(4)	0.0127(8)
Al3	0.500(5) Al	0.5000	0.3019(4)	0.4908(11)	0.0119(19)
Al4	Al	0.5000	0.0542(2)	0.3214(4)	0.0166(10)
Si5	0.500(5) Si	0.0000	0.0487(4)	0.3101(8)	0.0063(17)
B5	0.500(5) B	0.0000	0.014(2)	0.383(3)	0.024(7)
Al6	0.500(5) Al	0.5000	0.2435(4)	0.3469(8)	0.0088(14)
O1	O	0.0000	0.1944(5)	0.5906(9)	0.0094(19)
O2	O	0.5000	0.1825(5)	0.5510(10)	0.022(2)
O3	O	0.2405(8)	0.3112(4)	0.3692(6)	0.0221(18)
O4	O	0.2252(7)	0.0572(3)	0.4359(5)	0.0105(14)
O5	O	0.5000	0.0483(5)	0.7270(10)	0.0100(18)
O6	O	0.0000	−0.0492(5)	0.2451(10)	0.0106(17)
O7	O	0.0000	0.3593(6)	0.6785(12)	0.039(2)
O8	0.500(5) O	0.0000	0.1214(11)	0.163(2)	0.016(3)

Note: for Al1, Al2, Al4, and O1 to O7 U_{iso} represents U_{eq}.

$(0.10 \times 0.10 \times 0.03$ mm$^3)$ was previously excavated from a standard petrographic thin section using a micro-milling cutter (Medenbach, 1986) and was for this reason strongly strained. Originally data were collected using graphite monochromated $MoK\alpha$ (λ = 0.71073 Å) radiation and frame widths of 0.3° in ω, with 120 s used to acquire each frame. Subsequent reflection indexing and intensity integration failed probably because of strain-related poor reflection definition and occurrence of additional weak, diffuse super-structure reflections. As a consequence, a different data collection strategy was chosen. Short exposure times (30 s) were selected to reduce the peak shape to the inner, most intensive core, thus avoiding the diffuse tails. The resulting data could be indexed and successfully integrated. However, under these conditions, the super-structure reflections could no longer be resolved. Thus only diffractions characteristic of the average structure could be collected. All data were empirically corrected for anisotropic absorption using pseudo-ψ-scans of symmetrically equivalent reflections. Systematic absences

suggested three possible space groups: $Cmc2_1$ (No. 36), $Cmcm$ (No. 63), and $Ama2$ (No. 40). Data were reduced and corrected for Lorentz, polarization, and background effects using the program SAINT (Bruker, 1999). Scattering curves for neutral atoms, together with anomalous dispersion corrections, were used. The Bruker SHELXTL Version 5.1 (Bruker, 1997) system of programs was used for solution and refinement of the crystal structure on the basis of F^2. Subsequent attempts to solve the structure in all three suggested space groups indicated that the observed average structure possesses the acentric space group $Cmc2_1$ (No. 36). Direct methods were utilised to locate the fully occupied cation sites. By subsequent difference-Fourier summations the oxygen atoms and partly occupied cation sites were determined. At this stage the polysomatic character of the structure was noticed and constrained occupancies of atomic positions, which were different in both modules, were refined. In the final least-squares cycles all fully occupied sites were refined with anisotropic displacement parameters. Partially occupied sites were kept isotropic. The Flack x = 0.14(48) parameter, indicating possible twinning by the inversion operation, is not meaningful due to the large associated standard deviation. Atomic coordinates and occupancies, isotropic displacement parameters, and selected interatomic distances are summarised in Tables 3 and 4.

Boromullite was analysed with a Cameca SX-100 electron microprobe at the University of Maine using wavelength-dispersive spectroscopy (WDS) using the method developed for analysing boralsilite (Grew *et al.*, 2008), which is summarised here. Each spot was analysed using Cameca's PeakSight software for B at 5 kV accelerating voltage and 40 nA beam current and for Mg, Al, Si, Ca, Ti, Mn, and Fe at 15 kV accelerating voltage and 10 nA beam current. The beam was focused for all elements. Analysis for B was done in peak-area mode with a Mo-B$_4$C (200 Å) synthetic crystal because the B peak is broad and asymmetrical; peak integration was carried

Table 4. Bond lengths (Å) and angles (°) for boromullite.

Al1	Distance	Angles				
O2	1.854(6)					
O5	1.867(6)	81.4(2)				
O1	1.886(5)	100.7(3)	177.2 (4)			
O4	1.934(5)	86.9(3)	92.0(3)	90.1(3)		
O3_$10	1.941(6)	95.2(3)	92.2(3)	85.7(3)	175.6(2)	
O6_$12	1.944(6)	175.0(5)	97.3(4)	80.8(2)	88.4(3)	89.7(3)
		O2	O5	O1	O4	O3_$10

Al2	Distance	Angles		
O7	1.687(10)			
O3	1.689(5)	114.4(2)		
O3_$5	1.689(5)	114.4(2)	109.0(4)	
O1	1.724(7)	97.7(4)	110.5 (3)	110.5 (3)
		O7	O3	O3_$5

Al3	Distance	Angles		
O8_$10	1.753(19)			
O3	1.759(7)	110.4(4)		
O3_$6	1.759(7)	110.4(4)	115.1(6)	
O2	1.853(9)	116.7(8)	102.1(3)	102.1(3)
		O8_$10	O3	O3_$6

Al4	Distance	Angles		
O7_$2	1.701(9)			
O5_$11	1.703(7)	114.64(4)		
O4	1.801(4)	107.2(2)	103.4(2)	
O4_$6	1.801(4)	107.2(2)	103.4(2)	121.5(3)
		O7_$2	O5_$11	O4

Si5	Distance	Angles		
O6	1.554(8)			
O8	1.570(19)	115.3(7)		
O4_$5	1.615(5)	105.5(4)	112.0(5)	
O4	1.615(5)	105.5(4)	112.0(5)	105.8(5)
		O6	O8	O4_$5

B5	Distance	Angles	
O6	1.42(2)		
O4_$5	1.498(14)	119.4(9)	
O4	1.498(14)	119.4(9)	118.5 (1.7)
		O6	O4_$5

Al6	Distance	Angles			
O3	1.807(5)				
O3_$6	1.807(5)	110.4(4)			
O2	1.815(9)	101.7(3)	101.7(3)		
O7_$2	2.014(10)	119.5(3)	119.5(3)	99.6 (4)	
O1_$2	2.177(9)	81.0(3)	81.0(3)	175.0(4)	75.5(3)
		O3	O3_$6	O2	O7_$2

Symmetry codes: $2: $−x + 1/2, −y + 1/2, z − 1/2$; $5: $−x, y, z$; $6: $−x + 1, y, z$; $10: $−x + 1/2, −y + 1/2, z + 1/2$; $11: $−x + 1, −y, z − 1/2$; $12: $−x, −y, z + 1/2$.

out over 1000 steps, spanning wavelengths 60 to 78 Å. An interval surrounding the peak was scanned; the non-peak areas were used as background and regressed to determine the background contribution under the peak. The B$K\alpha$ peak using a 200 Å, Mo-B$_4$C crystal is asymmetric: on boralsilite it was found to have 2.5 times higher background on the short wavelength side than on the long wave-length side. The background in the B$K\alpha$ interval increases markedly with SiO$_2$ content at wavelengths that would also affect the low wavelength side of the B$K\alpha$ peak. Higher SiO$_2$ content of the standard compared to boromullite may lead to an over estimate of B$_2$O$_3$, but quantifying these interferences is difficult. Equally difficult to quantify is the impact of a peak at approximately 67 Å found in scans

of minerals lacking B. It is unrelated to any specific interference and may be caused by fluorescence of B from the Mo-B_4C crystal (McGee & Anovitz, 1996). The other constituents were measured in peak-height mode. Backgrounds for all constituents were measured at each analytical spot. The following minerals served as standards: elbaite (B$K\alpha$, sample 98144, Dyar *et al.*, 2001 using B from the crystal-structure refinement and the University of Maine electron microprobe analysis for the other constituents), diopside (Mg$K\alpha$, Ca$K\alpha$), kyanite (Al$K\alpha$, Si$K\alpha$), rutile (Ti$K\alpha$), rhodonite (Mn$K\alpha$), and almandine (Fe$K\alpha$). Data were processed using the X-Phi correction of Merlet (1994).

Additional analyses of boromullite were obtained at the Electron Microscopy Unit, The Australian National University, using a JEOL 6400 SEM and energy dispersive spectrometry (EDS; Oxford ISIS EDXA detector). Operating conditions were 15kV accelerating voltage and 1 nA beam current at a working distance of 39 mm. Natural mineral and oxide standards were used to calibrate the EDS system and analysis totals were adjusted throughout analytical sessions to yield 100 wt.% for anhydrous and B-free minerals (in these samples, sillimanite and andalusite) through the use of a Faraday Cup. Eighty seconds of live time were used for each analysis and ZAF (atomic number, absorption, fluorescence) matrix corrections were employed using Link Semquant software. Backscattered electron (BSE) images were obtained using a Hitachi 4300 SE/N (Schottky Field Emission SEM) operating at beam conditions of 15 kV and 0.6 nA and a working distance of 15 mm.

Crystal structure

The refined average structure model indicates two superimposed modules (Fig. 2). Module 1 has the topology and stoichiometry of sillimanite and carries all the Si but none of the B, *i.e.*, $Al_4Si_2O_{10}$. Module 2 is a type of mullite defect structure (*e.g.*, Angel *et al.*, 1991; Balzar & Ledbetter, 1993; Fischer *et al.*, 1994) in which Si is replaced by B in triangular coordination and by Al in tetrahedral coordination, *i.e.*, Al_5BO_9. Instead of the uninterrupted tetrahedral Si-Al chains filling the channels between the columns of edge-sharing Al octahedra as in sillimanite, every other Al tetrahedron flips into the adjacent channel in domain 2. In the investigated grain, module 1 and module 2 are present in equal proportions.

Module 2 is structurally identical to the synthetic compound Al_5BO_9 described by Sokolova *et al.* (1978). The structures for $Al_{18}B_4O_{33}$ reported by Ihara *et al.* (1980) and Garsche *et al.* (1991) are identical to that for Al_5BO_9; the small deviation from stoichiometry is attributed to B replacing some Al in tetrahedral coordination.

The diffraction pattern of boromullite shows additional weak and diffuse (smeared) reflections, which could not be indexed because of their poor definition. These reflections are probably indicative of order between the coherent modules shown in Fig. 2. All observations are in line
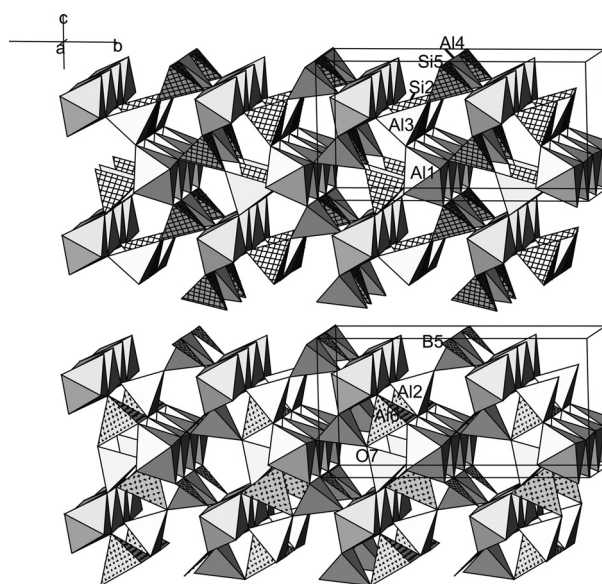

Fig. 2. The polysomatic boromullite structure comprises a sillimanite module (Al1, Si2, Al3, Al4, and Si5) and an Al_5BO_9 module (Al1, Al2, Al4, B5, Al6). O7 is shared by three tetrahedra. Structural drawings were prepared with ATOMS by Shape Software (2006).

with the interpretation of a polysomatic series between sillimanite and Al_5BO_9. Electron microprobe analysis gave a composition near $Al_9BSi_2O_{19}$, *i.e.*, about halfway between sillimanite and Al_5BO_9 (Fig. 1), which is confirmed by site occupation refinement, and both indicate a 1:1 polysome. Because the diffuse superstructure reflections could not be analysed, the refined structure model represents a disordered 1:1 polysome. There is no information on the dimensionality of the stacking or on stacking axis (*a*, *b* or *c*).

There are three cation sites both modules have in common: octahedral Al1 and tetrahedral Al4 and (Si, Al)2 (Fig. 2). The last site is occupied by Si in the sillimanite module and by Al in the Al_5BO_9 module, which explains why the mean (Si, Al)2-O distance of 1.696 Å (Table 5) is intermediate between Si-O and Al-O. Tetrahedral Al3 occurs only in the sillimanite module and flips into the adjacent channel (Al6) in the Al_5BO_9 module. Si5 is also characteristic of the sillimanite module. Instead, in the Al_5BO_9 module boron (B5) centres one triangular face of the former $Si5O_4$ tetrahedron. The oxygen sites O1 to O7 are also common to both modules. O8 (half occupied) occurs in the sillimanite module only and connects the tetrahedra Si5 and Al3, which are both empty in the Al_5BO_9 module. A peculiar bonding situation is found for O7 connecting three Al tetrahedra (Al2, Al4, and Al6) in the Al_5BO_9 module. A simple bond strength approach indicates that O7 balances $3 \times {}^3/_4$ cation charges and is therefore formally overbonded. This situation, characteristic of mullite-like structures (*e.g.*, Angel *et al.*, 1991; Balzar & Ledbetter, 1993; Fischer *et al.*, 1994), also explains why Si occupancy of the fifth site in the Al_5BO_9 module is negligible: the presence of Si would exacerbate overbonding of O7.

In previous structure refinements of Al_5BO_9 [or $Al_5(BO_3)O_6$] and $Al_{18}B_4O_{33}$ (Sokolova *et al.*, 1978; Ihara

Table 5. Labeling and mean M-O bond lengths for corresponding cation sites in boromullite, sillimanite, and Al_5BO_9.

Boromullite (this study)		Sillimanite (Bish & Burnham, 1992)		Al_5BO_9 (Sokolova *et al.*, 1978)	
Site / occupancy	Mean bond length (Å)	Site / occupancy	Mean bond length (Å)	Site / occupancy	Mean bond length (Å)*
^{VI}Al1	1.904	^{VI}Al1	1.912	^{VI}Al1	1.901
^{IV}(Si, Al)2	1.697	^{IV}Si1	1.633	^{IV}Al4	1.748
^{IV}Al3 0.5 Al	1.781	^{IV}Al2	1.754		
^{IV}Al4	1.752	^{IV}Al2	1.754	^{IV}Al3	1.793
^{IV}Si5 0.5 Si	1.589	^{IV}Si1	1.633		
^{III}B5 0.5 B	1.472			^{III}B1	1.374
^{IV}Al6 0.5 Al	1.861			^{IV}Al2	1.791

Note: *Calculated from the atomic coordinates given in Table 2 of Sokolova *et al.* (1978).

et al., 1980; Garsche *et al.*, 1991) two Al sites Al4 and Al6 (according to our labeling) were described as five-fold coordinated. This is generally correct, however, a 4+1 coordination is probably a better description of the Al environment. In Al_5BO_9 (Sokolova *et al.*, 1978), *e.g.*, Al2 exhibits four bonds to oxygen below 1.85 Å and a fifth bond is 2.25 Å. In our description of the boromullite structure we neglect the long Al-O bonds and prefer a description of both distorted polyhedra as tetrahedra. Another reason is that Al4 (our labeling) occurs also in the sillimanite module and is there tetrahedrally coordinated (Bish & Burnham, 1992).

The average structure of boromullite has the same space group ($Cmc2_1$; No. 36) and corresponding cell dimensions ($a = 5.7168(15)$, $b = 15.023(5)$, $c = 7.675(3)$ Å) as Al_5BO_9 (Sokolova *et al.*, 1978). Thus, the sillimanite module is described with lower symmetry and doubled *a*-axis (corresponding to *b* in boromullite) than the true sillimanite structure (space group $Pbnm$ (No: 62), $a = 7.4841(3)$, $b = 7.6720(3)$, $c = 5.7707(2)$ Å (Bish & Burnham, 1992). In addition, it should be noted that the sillimanite module cannot be derived from the sillimanite structure ($Pbnm$) according to a group-subgroup relationship because $Cmc2_1$ is not a subgroup of $Pbnm$. Table 5 relates cation positions in the two modules of boromullite to those of the end-member structures sillimanite (Bish & Burnham, 1992) and Al_5BO_9 (Sokolova *et al.*, 1978). Fischer & Schneider (2008) give the position of boromullite in the family of mullite-type structures.

Physical and optical properties of boromullite

Boromullite most commonly forms very fine intergrowths with sillimanite that can only be resolved in back-scattered electron images (*e.g.*, Grew *et al.*, 2008). Sample 2006-MST22 is exceptional; here boromullite tends to form prisms or bundles of prisms up to 0.4 mm long; some bundles are splayed, *e.g.*, the holotype prism (Fig. 3). Nonetheless, even these prisms are not free of intergrown sillimanite, which appears as slightly lighter patches in a dark matrix (Fig. 3b). No cleavage is evident in boromullite, which is brittle. Density calculated with empirical formula
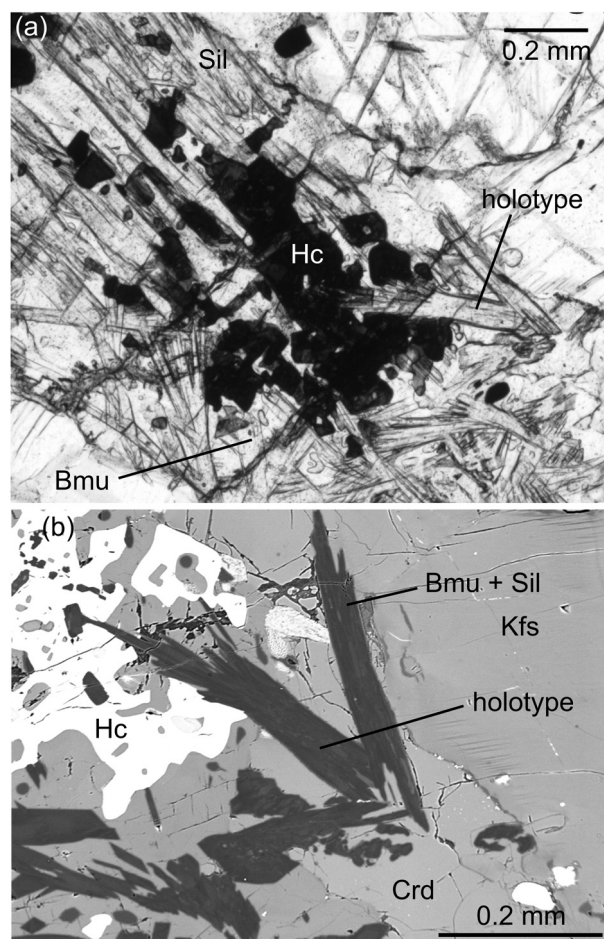

Fig. 3. Holotype boromullite prism in thin section 2006-MST22a. a) Photomicrograph, plane polarised light. b) Back-scattered electron image. Abbreviations: Bmu – boromullite, Crd – cordierite, Hc – hercynite, Kfs – K-feldspar, Sil – sillimanite.

is 3.081 g/cm^3. Other physical properties could not be determined.

Boromullite is colourless and transparent, biaxial (+), n_x 1.627(1), n_y 1.634(1), n_z 1.649(1) (589 nm). $2V_Z$ (meas) = 57(2)°, $2V_Z$ (calc) = 69(12)°; *i.e.*, the
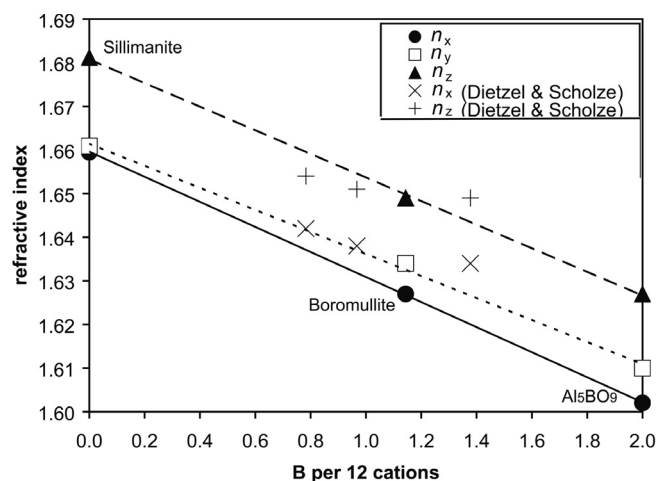
Fig. 4. Refractive indices of sillimanite (Bloss *et al.*, 1983), boromullite (this study) and Al_5BO_9 (Scholze, 1956). Uncertainties of ± 0.001 (Scholze, 1956; this paper; Bloss *et al.*, 1983, gave sillimanite indices to 4 significant figures, but did not specify the uncertainties) are smaller than the symbols. Lines are least-squares fits to these data. The crosses are for the "boron-mullites" described by Dietzel & Scholze (1955).

measured and calculated $2V$ agree within the given uncertainties. The calculated $2V$ has a low precision because the precision for the indices is only ± 0.001 and the birefringence is not particularly high.

The refractive indices are virtually collinear as a function of B content (Fig. 4) with precise optical measurements reported for sillimanite (Bloss *et al.*, 1983) and Al_5BO_9 (Scholze, 1956). The n_z values reported by Dietzel & Scholze (1955) for intermediate compositions fit less well, and their n_x values are consistently too high, possibly due to their failure to resolve n_x and n_y.

No dispersion or pleochroism could be detected.

Chemical composition and compatibility index of boromullite

Boromullite is nearly pure boroaluminosilicate with minor MgO and FeO; other constituents are present at the limits of detection using either WDS or EDS (Fig. 5; Table 6). Because the modules differ in oxygen content but not in cation content, we have normalised formulae to a given number of cations; a 12-cation basis was chosen to give integral coefficients in the ideal formula, $Al_9BSi_2O_{19}$, for a 1:1 mix of $Al_{10}B_2O_{18}$ and $Al_8Si_4O_{20}$. Boromullite is compositionally heterogeneous on a very fine scale in 8 of the 9 samples, and thus each spot analysis has to be treated individually instead being averaged (Grew *et al.*, 2008; this paper, Fig. 5, 6). The situation in sample 2006-MST22 is much improved; the mineral forms prisms or bundles of prisms sufficiently large and homogeneous to average analyses in 17 areas on 15 grains in three thin sections cut from this sample. Nonetheless, standard deviations are commonly high (Table 6), indicating considerable heterogeneity, presumably intergrown sillimanite (Fig. 3b).

Compositions plot close to the join between Al_2SiO_5 (sillimanite) and Al_5BO_9 (Fig. 1, 6). The coarsest grain analysed in sample 2006-MST22 has a composition close to the midpoint, *i.e.*, $Al_9BSi_2O_{19}$. Boron-poor compositions approach sillimanite (Grew *et al.*, 2008; this paper, Fig. 6). However, we cannot exclude the possibility that the electron beam was intersecting sillimanite intergrown with boromullite (*e.g.*, Fig. 3b), *i.e.*, there could be a compositional gap between boromullite and sillimanite as wide as that shown in Fig. 1. Grew *et al.* (2008) calculated the maximum B content in three samples from a least squares fit of individual analyses SiO_2 16.5, Al_2O_3 76.2, B_2O_3 6.5 (erroneously given as 7.1 wt.% in Grew *et al.*), Sum 99.2 wt.%, *i.e.*, $Al_{9.17}Si_{1.68}B_{1.15}O_{18.84}$ (per 12 cations), which is close to the holotype in B content (Table 6), whereas spots analysed by EDS gave lower SiO_2 contents (Fig. 6), implying an even higher content of B_2O_3, but one still less than boromullite in an atoll around werdingite (Fig. 7b, d). FeO and MgO contents do not vary with SiO_2 content (Fig. 5), implying that these constituents are incorporated in both modules. Boromullite FeO contents overlap with contents of Fe (as FeO) found in sillimanite (10–12 analyses) in Mount Stafford B-rich metapelites; these range from below detection (~ 0.2 wt.%) to ~ 0.5 wt.%.

The Gladstone – Dale relation (Mandarino, 1981) gives a compatibility index $1 - (K_P/K_C) = 0.005$ (superior, with k value of $Al_2O_3 = 0.207$), $= -0.119$ (poor, with k value of Al_2O_3 for nesosilicates = 0.176) for sample 2006-MST22, section a/area 2/grain 2. Both k values for Al_2O_3 have also been applied to two other nesosilicates: mullite from Mull (Bowen *et al.*, 1924; Agrell & Smith, 1960; Deer *et al.*, 1982, Table 67, #5) and sillimanite from Brandywine (Aramaki & Roy, 1963; Deer *et al.*, 1982, Table 66, #3, excluding H_2O): the "normal" k value gave superior compatibilities of 0.009 and 0.007, respectively, but the "nesosilicate" k value gave poor compatibilities of -0.105 and -0.098, respectively. This "nesosilicate" k value (Mandarino, 1981) seems to be inappropriate for high Al_2O_3 contents in nesosilicates. Bloss *et al.* (1983) reported that $k = 0.207$ for Al_2O_3 and $k = 0.301$ for Mn_2O_3 gave better compatibilities for andalusite and kanonaite than $k = 0.176$ for Al_2O_3 and $k = 0.256$ for Mn_2O_3, but neither gave as good compatibilities as their own set of k values for the major constituents SiO_2, Al_2O_3, Mn_2O_3 and Fe_2O_3 in andalusite and kanonaite.

Synthetic analogues

"Boron-mullites" have been synthesised in simple experimental systems (B_2O_3-Al_2O_3-SiO_2 ± H_2O ± MgO) at temperatures above 500 °C and pressures up to nearly 8 kbar (*e.g.*, Werding & Schreyer, 1996; Grew *et al.*, 2008; Griesser *et al.*, 2008). In addition, by the dry melting of a tourmaline-bearing granite at $T = 841$–1100 °C and $P = 1$ bar, Chorlton (1973) and Chorlton & Martin (1978) synthesised an acicular phase having up to five lines characteristic of mullite in its X-ray powder pattern and showing weak blue-green pleochroism.
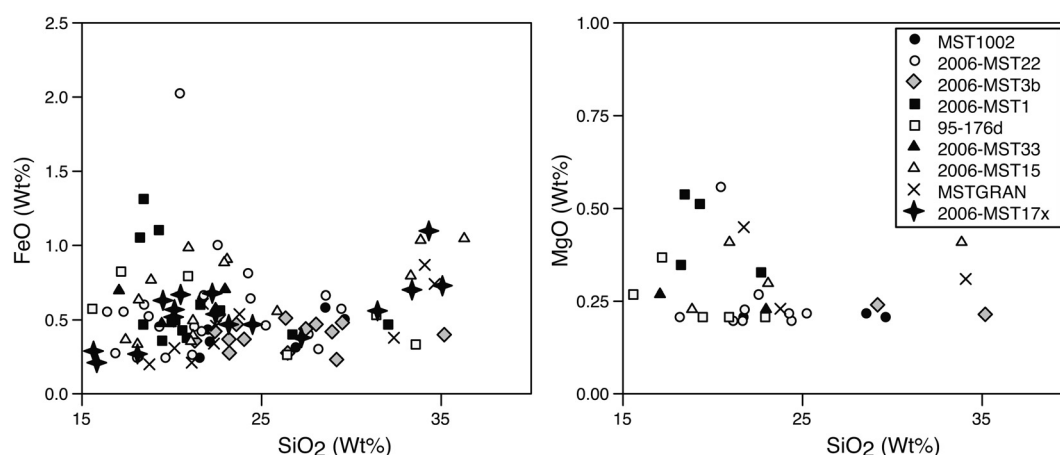
Fig. 5. FeO, MgO and SiO₂ contents of boromullite measured in 9 samples with the electron microprobe using energy-dispersive spectroscopy (individual analyses). There are fewer points for MgO because this constituent is commonly below the limit of detection. Fe is presumed to be divalent in boromullite.

Table 6. Representative compositions of boromullite in sample 2006-MST22.

Grain*	a/2/2	c/2/1	b/3/2	b/5/2	a/2/4
Number**	11	7	4	15	7
	SREF	atoll	min B	mid B	max B
Wt.%					
SiO₂	19.01(1.12)	13.75(0.40)	23.36(1.07)	21.54(0.88)	17.73(0.38)
TiO₂	0.01(0.02)	0.03(0.02)	0.04(0.03)	0.02(0.01)	0.02(0.01)
B₂O₃	6.52(0.75)	7.79(0.62)	4.45(1.49)	5.52(1.35)	6.99(0.88)
Al2O₃	74.10(0.95)	77.95(0.28)	71.00(0.98)	72.22(0.79)	74.66(0.68)
MgO	0.07(0.03)	0.04(0.00)	0.05(0.00)	0.08(0.06)	0.20(0.14)
CaO	0.00(0.02)	0.00(0.01)	0.01(0.00)	0.01(0.01)	0.04(0.01)
MnO	0.01(0.04)	0.01(0.03)	0.01(0.02)	0.01(0.03)	0.00(0.02)
FeO	0.40(0.08)	0.42(0.04)	0.34(0.03)	0.45(0.18)	0.44(0.27)
Sum	100.12	99.98	99.26	99.84	100.09
Formula per 12 cations					
Si	1.932	1.381	2.435	2.214	1.796
Ti	0.001	0.002	0.003	0.001	0.002
B	1.144	1.351	0.800	0.980	1.221
Al	8.878	9.225	8.722	8.751	8.910
Mg	0.011	0.007	0.008	0.012	0.031
Ca	0.000	0.000	0.001	0.001	0.004
Mn	0.000	0.001	0.001	0.001	0.000
Fe	0.034	0.035	0.030	0.039	0.037
Sum	12.000	12.000	12.000	12.000	12.000
O	18.944	18.670	19.199	19.081	18.863

Notes: All Fe as FeO. Analyses by wavelength-dispersive spectroscopy. *Grains designated by section/area/individual grain. **Number of individual analyses used in average. SREF: holotype prism used for optical measurements and crystal structure refinement. Atoll: see Fig. 7b, d.

However, chemical analyses of synthetic "boron-mullites" are relatively few (Letort, 1952; Dietzel & Scholze, 1955; Gelsdorf *et al.*, 1958; Werding & Schreyer, 1992; Grew *et al.*, 2008). The compositions plot in two linear trends (Buick *et al.*, 2007b; Grew *et al.*, 2008): (1) material synthesised from gels at 930–1050 °C, including the compound $Al_8B_2Si_2O_{19}$, and (2) material synthesised in association with an anhydrous B_2O_3-Al_2O_3-SiO_2 melt, either from reaction of mullite with the melt at 1200 °C or directly precipitated from the melt on the liq-

uidus at 1520–1600 °C. Plotted points of the latter lie on the join Al_5BO_9–Al_2SiO_5 and three of the four compositions overlap with boromullite (Fig. 1). Gelsdorf *et al.* (1958) also reported cell parameters for one of their "boron-mullites" (not the analysed one): $a = 15.00$ Å, $b = 7.67$ Å, $c = 5.66$ Å, *i.e.*, *a* and *c* doubled relative to mullite, but close to those for boromullite allowing for the different unit cell orientation. A third indication that this synthetic "boron-mullite" and boromullite could be analogues is the similarity in the n_z refractive indices (Fig. 4); agreement of
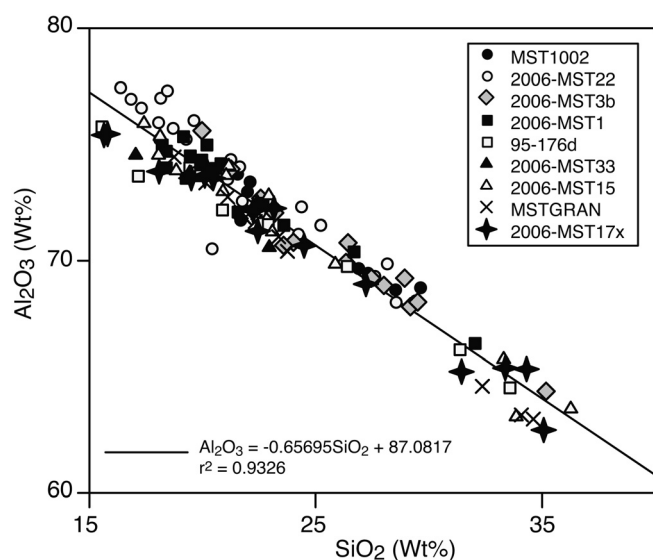
Fig. 6. Al_2O_3 and SiO_2 contents of boromullite measured in 9 samples with the electron microprobe using energy-dispersive spectroscopy (individual analyses). The least squares regression line passes close to the ideal values for $Al_9BSi_2O_{19}$, *i.e.*, 74.22 wt.% Al_2O_3 (*vs.* 74.75 wt.% at 19.58 wt.% SiO_2) and Al_2SiO_5, *i.e.*, 62.72 wt.% Al_2O_3 (*vs.* 62.92 wt.% at 37.08 wt.% SiO_2).
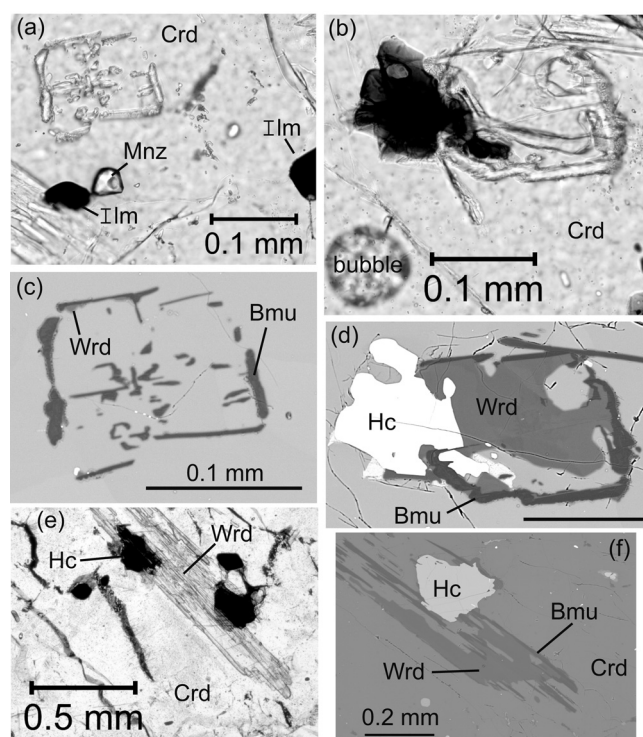

Fig. 7. Boromullite replacement of werdingite in sample 2006-MST22. (a) Photomicrograph of a boromullite atoll in cordierite matrix; a second aggregate consisting of boromullite and/or werdingite in lower left, section 2006-MST22c. Plane polarised light. (b) Photomicrograph of a second boromullite atoll in cordierite matrix, 2006-MST22c (analysis in Table 6). Plane polarised light. (c) Backscattered electron image of atoll in (a). Narrow rims of werdingite are present locally on inside of boromullite atoll. (d) Back-scattered electron image of atoll in (b). Scale bar is 0.1 mm. (e) Photomicrograph of an embayed werdingite prism in section 2006-MST22a. Plane polarised light. (f) Back-scattered electron image of this prism showing boromullite overgrowth. Abbreviations: Bmu – boromullite, Crd – cordierite, Hc – hercynite, Ilm – ilmenite, Mnz – monazite, Sil – sillimanite, Wrd – werdingite.

the n_x indices is much less good, possibly because indices between n_x and n_y were measured instead of the n_x index. Overall, full confirmation that "boron-mullite" synthesised with B_2O_3-Al_2O_3-SiO_2 melts is an analogue of boromullite would require crystal structure refinement of the synthetics to demonstrate that they are also polysomes composed of Al_5BO_9 and Al_2SiO_5 modules.

Griesser *et al.* (2008) synthesised two series of B-substituted mullites at 950 and 1300 °C: one containing 60 mole% Al_2O_3 and 0–20 mole% B_2O_3 and the other, 70 mole% Al_2O_3 and 0–15 mole% B_2O_3 (*cf.* 5.6–10.1 mole% B_2O_3 and 60.0–69.1 mole% Al_2O_3 in boromullite); higher B_2O_3 contents yielded aluminoborate and SiO_2. Doubling of cell parameters was not reported in the Rietveld refinements. The cell parameters of the B-substituted mullites either decrease or remain unchanged with increasing B content. Comparison of the cell parameters of sillimanite, boromullite and aluminoborate suggest that the *a* cell parameter and cell volume decrease with increasing B, but the *b* and *c* parameters actually increase slightly (Fig. 8). It is possible that Griesser *et al.* (2008) have synthesised a B-bearing mullite distinct from boromullite, but their chemical and X-ray data are not sufficient to demonstrate conclusively that boromullite is absent from their synthetics.

Paragenesis of boromullite and associated borosilicates

The Mount Stafford area comprises Proterozoic metasedimentary and metagranitic rocks of the Arunta Region (Fig. 9). Metamorphic conditions at Mount Stafford in-

crease from the lower amphibolite-facies ($T \leq 620$ °C, $P \leq 2.3$–2.8 kbar in zone 1) to the granulite-facies (810 °C $\approx T \geq 775$–785 °C, $P = 3.3$–4 kbar in zone 4) over a distance of only some 10 km (Clarke *et al.*, 1990; Vernon *et al.*, 1990; Collins & Vernon, 1991; Greenfield *et al.*, 1998; White *et al.*, 2003). Rubatto *et al.* (2006) reported SHRIMP (sensitive high-resolution ion microprobe) U–Pb ages of metamorphic zircon rims and monazite that dated granulite-facies metamorphism between ~ 1795 and 1805 Ma, and intrusion of the granite east of the metamorphic rocks (Fig. 9) at 1802 ± 3 Ma, *i.e.*, coeval with metamorphism. Rubatto *et al.* (2006) concluded that their geochronological results are consistent with the complex field relationships between granite and granulites described by previous investigators and with the hypothesis that magmatism and metamorphism at Mount Stafford are interrelated, and expressed doubts that the granite could be the heat source for the high-temperature metamorphism.
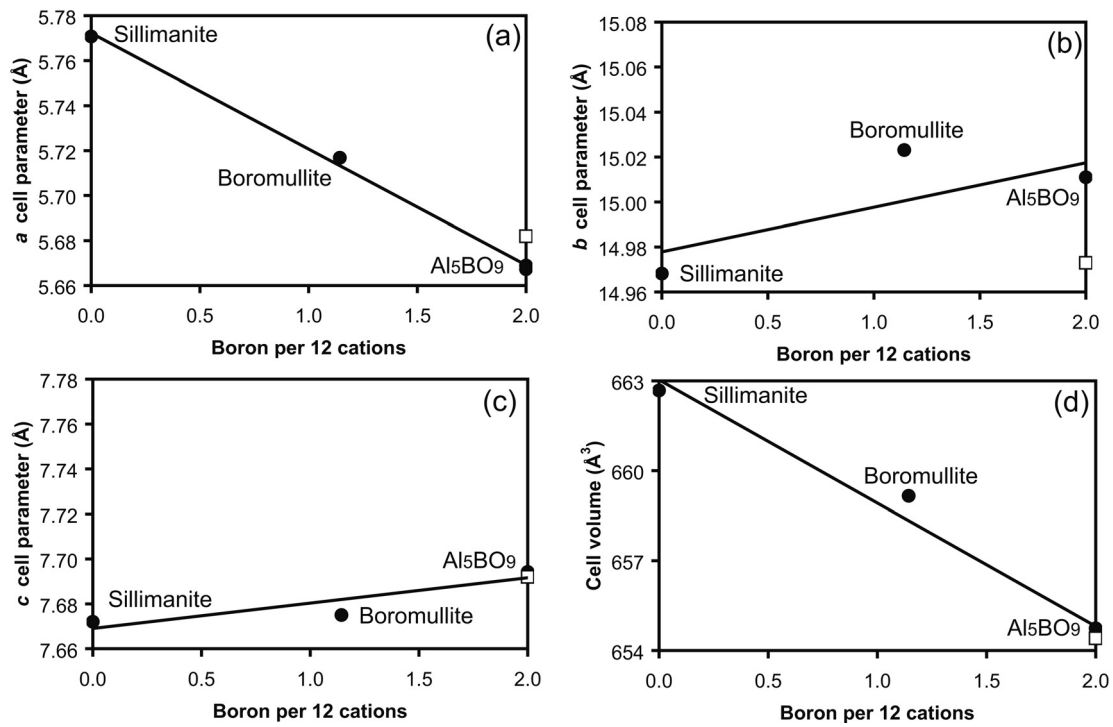
Fig. 8. Variation of cell parameters for sillimanite (Bish & Burnham, 1992), boromullite (this paper), and Al_5BO_9 or $Al_{18}B_4O_{33}$ (Sokolova *et al.*, 1978; Ihara *et al.*, 1980; Garsche *et al.*, 1991). Lines are least squares fits excluding the Ihara *et al.* (1980) data (open squares) because of the larger reported errors. Cell parameters of sillimanite, Al_5BO_9 or $Al_{18}B_4O_{33}$ were interchanged or doubled as necessary for direct comparison with boromullite.
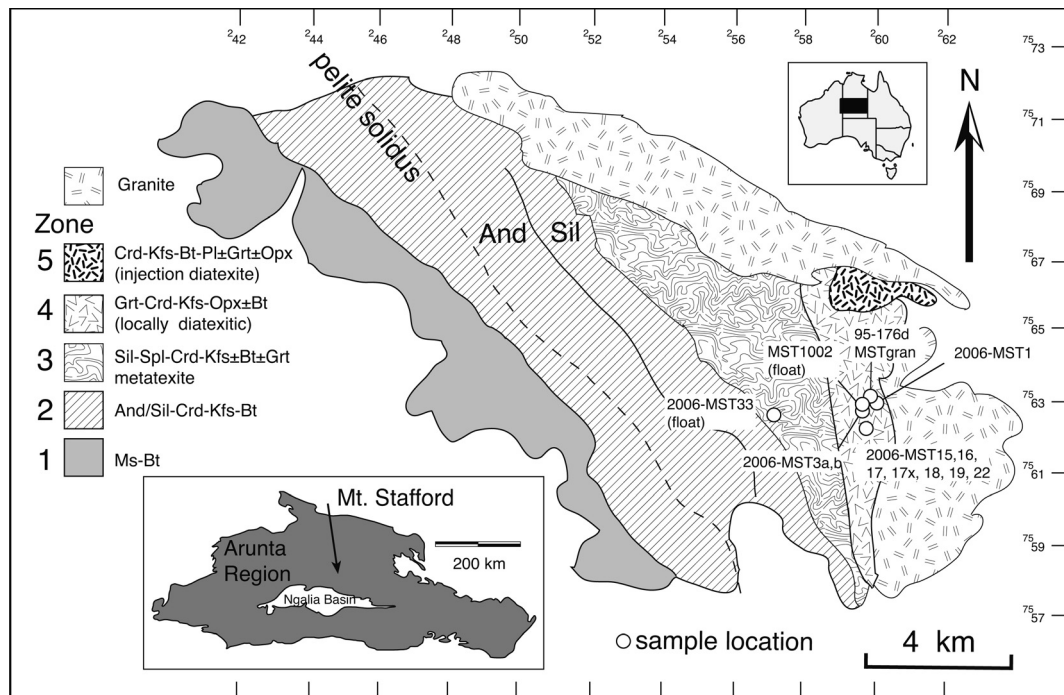
Fig. 9. Map of the metamorphic zones in the Mount Stafford area (modified from Greenfield *et al.*, 1998; Rubatto *et al.*, 2006) showing location of 14 samples containing boromullite.
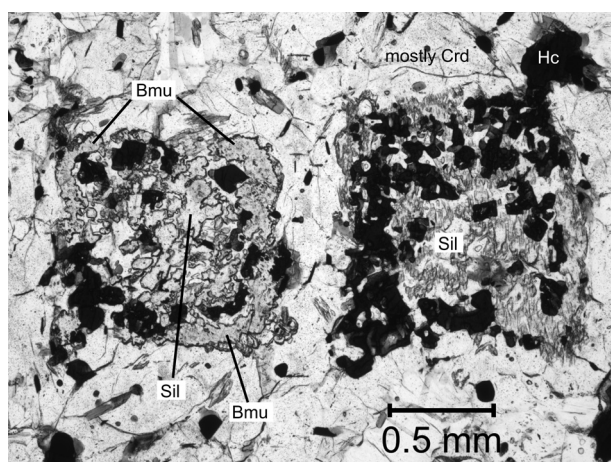
Fig. 10. Photomicrograph of two blocky sillimanite aggregates with abundant hercynite; one has partial overgrowth of boromullite. Thin section 2006-MST22a, plane polarised light. Abbreviations: Bmu – boromullite, Crd – cordierite, Hc – hercynite, Sil – sillimanite.

Tourmaline is found in zones 1–4, whereas boromullite, werdingite and its Fe-dominant analogue and grandidierite-ominelite, have been found *in situ* only in zone 4. However, float containing the three borosilicates has been found within zone 3. Because these finds are down slope from outcrops in zone 4, the presence of any of these borosilicates in zone 3 cannot be confirmed, and it appears likely their appearance coincided to a first approximation with the transition from zone 3 to zone 4.

Boromullite has been identified with EDS in 14 samples of metapelites, 8 of which contain abundant borosilicate minerals; the others contain only traces. Sillimanite, cordierite-sekaninaite and K-feldspar are abundant in all the sections, whereas biotite, hercynite and ilmenite are subordinate and quartz is rare. Both Fe- and Mg-dominant analogues of werdingite, grandidierite and cordierite are present in the boromullite-bearing rocks, *i.e.*, $X_{Mg} = Mg/(Mg + Fe) = 0.41$–$0.50$ (werdingite), 0.39–0.55 (grandidierite) and 0.38–0.54 (cordierite), and for simplicity we refer to the minerals of these three series by the names of the Mg end-members. Andalusite and plagioclase is present in a few sections. The most widespread accessories are monazite-(Ce), an apatite-group mineral and zircon.

The type sample (2006-MST22) is characterised by sillimanite aggregates pseudomorphic after andalusite, relics of which remain. Boromullite is sufficiently abundant and coarse-grained (to 0.4 mm, Fig. 3) to be recognised under the petrographic microscope; nonetheless its similarity to sillimanite makes identification a challenge. Boromullite prisms typically form fringes and bundles surrounding sillimanite aggregates (Fig. 10) or are found mixed with sillimanite. Even the relatively coarse boromullite prisms contain some intergrown sillimanite (Fig. 3b). Boromullite also forms narrow overgrowths of werdingite. When the length of the werdingite prism is at a high angle to the section, the overgrowths resemble atolls, *i.e.*, cordierite appears in the space now only partially occupied by werdin-

gite (Fig. 7a–d). When their length is at a low angle to the section, werdingite prisms appear embayed (Fig. 7e, f).

In most samples, boromullite forms microscopic intergrowths with sillimanite (*e.g.*, Grew *et al.*, 2008). The boromullite-sillimanite intergrowths are mostly found as a replacement of werdingite; in a few cases, they could also be replacing andalusite (Fig. 11a). The converse is suggested by werdingite surrounding a boromullite-sillimanite-cordierite aggregate in sample 2006-MST15 (Fig. 11b), but this texture could also have resulted from the breakdown of werdingite. Sillimanite and boromullite are commonly intergrown along a surface parallel to the prism length (*e.g.*, Fig. 11a, 11c, 12c), but intergrowths along surfaces across the prism length are also found (Fig. 12a); boralsilite and werdingite form similar ladderlike ("scalariform") intergrowths (Grew *et al.*, 1998a). In sample 2006-MST3a dark sub-micrometer lamellae in sillimanite appear to be boromullite (Fig. 12c, d); these could have resulted from breakdown of sillimanite containing a small proportion of Al_5BO_9 modules. Such ultrafine intergrowths could explain some compositions intermediate between Al_2SiO_5 and $Al_9BSi_2O_{19}$.

Quartz occurs in one boromullite-bearing sample (2006-MST17) as a string of three quite coarse ($\sim 1 \times 0.5$ mm) grains that wraps around one of the sillimanite pseudomorphs. Boromullite is found entirely enclosed in sillimanite (*e.g.*, Fig. 12a), and does not contact quartz or cordierite. No other borosilicate is present in this rock.

Small grains of tourmaline are enclosed in K-feldspar, andalusite and cordierite; the rounded ones appear to be relict (Fig. 11a), whereas the irregular ones look secondary. Sample 2006-MST33 is distinct from the others in that successive coronas of symplectitic tourmaline+hercynite and Al_2SiO_5+quartz intergrowths have developed between werdingite (partly replaced by boromullite and sillimanite) and cordierite (Fig. 13). Quartz in these intergrowths formed late and did not equilibrate with either werdingite or boromullite.

Textural relations suggest that werdingite is the first high-temperature borosilicate mineral to form in tourmaline-rich, metapelites by the following reaction involving anatexis:

Biotite + andalusite/sillimanite + tourmaline ± quartz =

werdingite + cordierite + hercynite + K-feldspar + liquid.

(1)
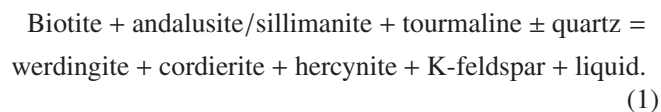
Although quartz was not found as a relatively coarse-grained matrix mineral in any of the werdingite-bearing samples (2006-MST2 contains grandidierite and quartz, but no werdingite), we suggest that it may have been a reactant by analogy to a similar reaction documented in B-poor Mt. Stafford metapelites. The assemblage werdingite + cordierite has not previously been reported, either in silica-undersaturated (Moore *et al.*, 1990; Grew *et al.*, 1997) or in silica-saturated rocks (Grew *et al.*, 1998b). Although the incompatibility of werdingite and cordierite is predicted in quartz-bearing rocks because the alternative assemblage grandidierite + sillimanite is widespread, the appearance
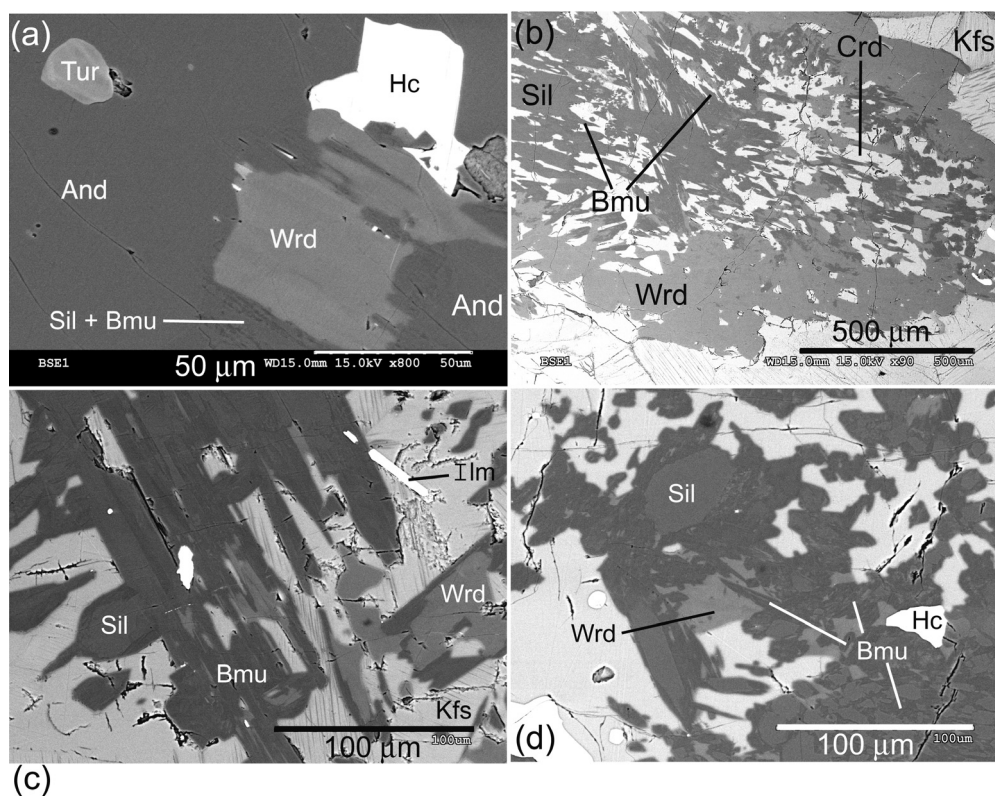
Fig. 11. Back-scattered images taken with FE-SEM of boromullite-sillimanite intergrowths and werdingite. (a) Intimate intergrowth of boromullite and Al_2SiO_5 (presumably sillimanite) around werdingite enclosed in andalusite. MST1002. (b) Boromullite-sillimanite mixed with cordierite and subordinate hercynite surrounded by werdingite. Sample 2006-MST15. (c) Relict werdingite in sillimanite-boromullite matrix. Sample 95-175D. (d) Relict werdingite in sillimanite-boromullite matrix. Sample 2006-MST1. Abbreviations: And – andalusite, Bmu – boromullite, Crd – cordierite, Hc – hercynite, Ilm – ilmenite, Kfs – K-feldspar, Sil – sillimanite, Tur – tourmaline, Wrd – werdingite.

of werdingite + cordierite in silica-undersaturated rocks is consistent with the compatibilities shown in Fig. 14.

Boromullite is later than werdingite. In sample MST1002, werdingite has reacted with andalusite to form boromullite + sillimanite (or a B-poor boromullite that later dissociated into boromullite + sillimanite). In sample 2006-MST22, the embayed appearance of werdingite suggests that it is a relict phase that was in the process of reacting with sillimanite to form boromullite, which has overgrown both sillimanite (Fig. 10) and werdingite (Fig. 7). There is no reaction evident in Fig. 14 that would introduce boromullite, so we suggest that the most plausible explanation for boromullite replacing werdingite is a shift in bulk composition associated with melt extraction. Of the components in the $(Fe, Mg)O-Al_2O_3-B_2O_3-SiO_2$ system, SiO_2 and B_2O_3 would most likely be incorporated in melt, enriching the restite in $(Fe, Mg)O$ and Al_2O_3. Decreasing SiO_2 and B_2O_3 can be viewed as a shift across B_2O_3 isopleths from the upper right to the lower left and "down" in Fig. 14. The assemblage boromullite + cordierite + sillimanite (light grey triangle, mostly hidden) lies at a lower SiO_2 and B_2O_3 than the assemblage werdingite + cordierite + sillimanite (darker grey triangle). Thus, a decrease in SiO_2 and B_2O_3 leads to the replacement of werdingite by boromullite. Expulsion of melt insured that the assemblages would escape rehydration, thereby preserving boromullite.

Textures indicate that grandidierite is also later than werdingite, and like boromullite, appears to be prograde, but the timing of grandidierite relative to boromullite is not evident because a reaction relationship has not been observed.

It is likely most of the melt left the rocks, because the assemblages show relatively little rehydration (Buick *et al.*, 2006, 2007a). Nonetheless, there is minor secondary tourmaline, including symplectite with hercynite, and what appears to be secondary biotite.

Pressure-temperature conditions for the borosilicate minerals

Tourmaline persisted to higher metamorphic grade in the Mount Stafford metapelitic rocks than in typical pelitic rocks containing only trace tourmaline and modest amounts of B, *e.g.* the Ryoke metamorphic belt (< 1 volume % tourmaline and 4–120 ppm B, Kawakami, 2001; 2004; Kawakami & Ikeda, 2003), for which the upper stability limit estimated for tourmaline (Fig. 15) could be representative. The majority of sub-solidus metapelitic rocks from Mount Stafford have similar B contents, and their high grade equivalents have even lower B contents and lack borosilicate minerals or contain but trace amounts (Buick
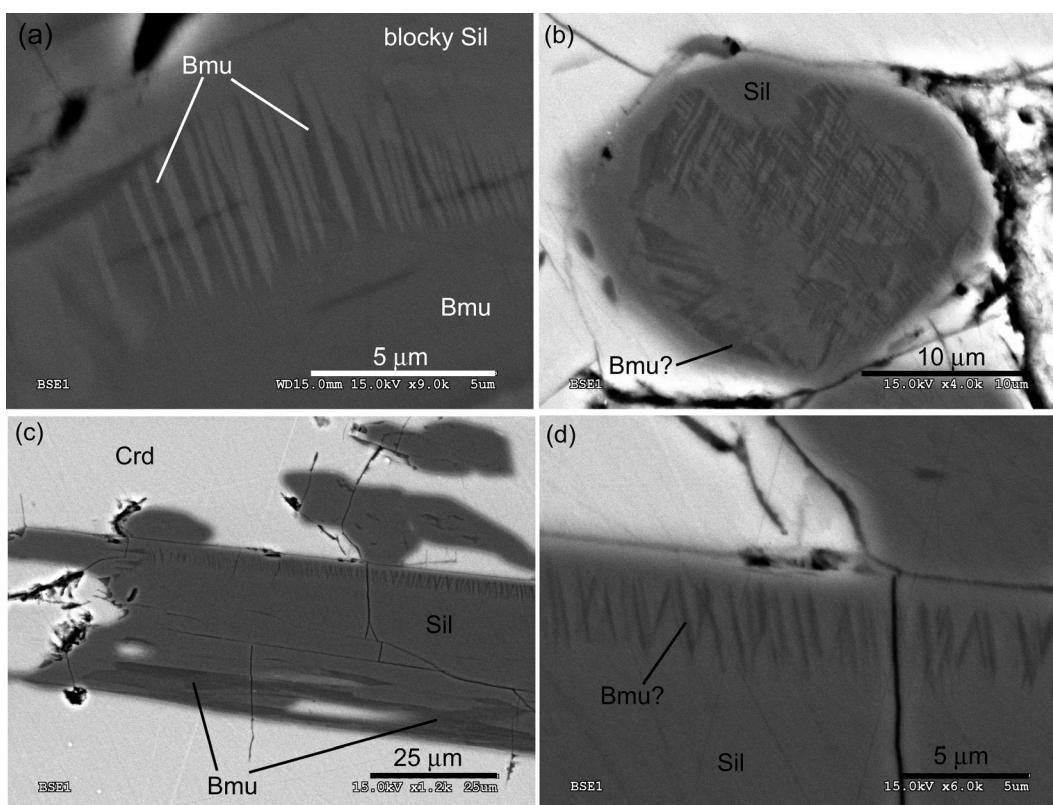
Fig. 12. Back-scattered electron images of sillimanite-boromullite intergrowths (a) Intergrowth in a patch of boromullite enclosed in a blocky sillimanite prism. Sample 2006-MST17. (b) Sample 2006-MST3a. (c) Sample 2006-MST3a, second area. (d) Enlargement of a portion of (c). Abbreviations: Bmu – boromullite, Crd – cordierite, Sil – sillimanite.
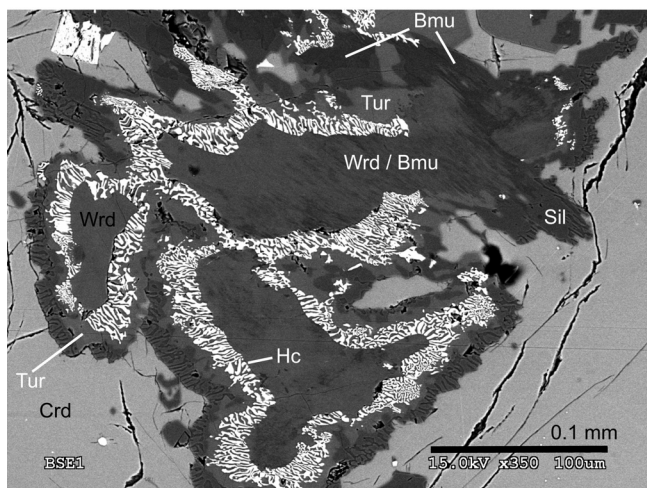

Fig. 13. Back-scattered electron image of werdingite surrounded by successive coronae of hercynite + tourmaline and Al_2SiO_5+quartz symplectite. Sample 2006-MST33. Abbreviations: Bmu – boromullite, Crd – cordierite, Hc – hercynite (in symplectite), Sil – sillimanite (in symplectite), Tur – tourmaline, Wrd – werdingite, Wrd / Bmu – werdingite partially replaced by boromullite.

et al., 2006, 2007a). Rare subsolidus metapelites contain large amounts of tourmaline (Spicer *et al.*, 2004) and are far richer in B (~ 2500–6500 ppm, Buick *et al.*, 2006, 2007a)

than the Ryoke metapelitic rocks. We suggest that tourmaline abundance prevented its loss in the early stages of melting, thereby allowing for its breakdown at higher temperatures to werdingite. Tourmaline could be stable with melts formed by anatexis of the Mount Stafford rocks to temperatures as high as 850 °C (Spicer *et al.*, 2004), *i.e.*, higher than the maximum estimated for zone 4.

Given that werdingite is restricted to zone 4, reaction 1 most likely took place near the boundary between zones 3 and 4 (Fig. 9), *i.e.*, at T = 775–785 °C, P = 3.3–4 kbar (Fig. 15 from White *et al.*, 2003), *i.e.*, within the synthesis field of the Mg end member (Werding & Schreyer, 1992).

Possible temperatures for boromullite formation at Mount Stafford are also constrained by the estimates for zone 4, *viz.* a minimum of 775–785 °C and a maximum of ~ 810 °C at P = 3.3–4 kbar (Greenfield *et al.*, 1998; White *et al.*, 2003). Werding & Schreyer (1996) reported a "boron-mullite" of unknown composition among the breakdown products of dumortierite, and suggested it could contain less B than the phase $Al_8B_2Si_2O_{19}$ (Fig. 14), *i.e.*, possibly a synthetic analogue of boromullite. The $P - T$ conditions inferred for boromullite exceed the stability of dumortierite determined by Werding & Schreyer (1996) in the B_2O_3-Al_2O_3-SiO_2-H_2O model system (Fig. 15). Given the presence of fluid and quartz among its breakdown products in the experiments, low H_2O activities and loss of quartz to anatectic melt would be expected to lower the breakdown temperature of dumortierite. Figure 14
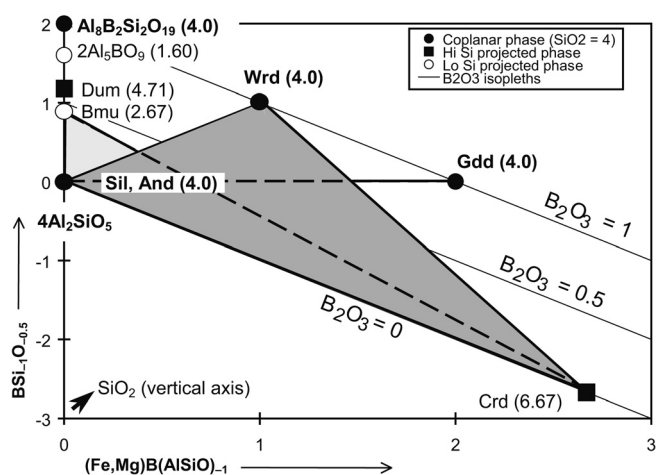
Fig. 14. Ideal compositions of boromullite ($Al_9BSi_2O_{19}$), $Al_8B_2Si_2O_{19}$, Al_5BO_9, dumortierite [$Al_{6.8}BSi_3O_{17.4}(OH)_{0.6}$], werdingite [$(Fe, Mg)_2Al_{14}B_4Si_4O_{37}$], grandidierite [$(Fe, Mg)Al_3BSiO_9$], aluminosilicates ($Al_2SiO_5$) and cordierite [$(Fe, Mg)_2Al_4Si_5O_{18}$] plotted in terms of vector components $(Fe, Mg)B(AlSiO)_{-1}$ and $BSi_{-1}O_{-0.5}$ added to or subtracted from Al_2SiO_5 with SiO_2 vertical (*cf.* Grew *et al.*, 1998a, Fig. 8) instead of traditional components $(Fe, Mg)O$-Al_2O_3-B_2O_3-SiO_2. Given the overlapping ranges for Mg/(Mg+Fe) ratio for werdingite (0.41–0.50). grandidierite (0.39–0.55) and cordierite (0.38–0.54) in samples containing boromullite from Mount Stafford, we have combined MgO and FeO into a single component, and for simplicity, we refer to the three ferro-magnesian minerals by the names of the Mg end-members. In the presence of quartz, the compositions can be projected onto the $(Fe, Mg)B(AlSiO)_{-1} - BSi_{-1}O_{-0.5}$ plane, and Sil + Gdd would be incompatible with Wrd + Crd. Abbreviations: And – andalusite, Bmu – boromullite, Crd – cordierite, Dum – dumortierite, Gdd – grandidierite, Sil – sillimanite, Wrd – werdingite.

shows that dumortierite is relatively SiO_2 rich compared to werdingite and grandidierite, and assemblages such as Dum + Wrd + Crd and Dum + Sil + Crd require higher bulk SiO_2 content than Wrd + Sil + Crd. The availability of Ti, which is incorporated in significant amounts in dumortierite (Werding & Schreyer, 1996; Grew, 1996), would have the opposite effect by stabilising dumortierite to higher temperature as it does biotite (Patiño Douce, 1993) or to lower bulk SiO_2 contents.

Could boromullite occur elsewhere?

The $P - T$ conditions inferred for boromullite formation at Mount Stafford are by no means unusual and boromullite is not restricted to rocks unusually rich in boron, observations that raise the question why boromullite has developed so extensively there and not elsewhere. In addition, boromullite is not restricted at Mount Stafford to silica-undersaturated rocks, suggesting the possibility of boromullite + quartz assemblages even though none has been found at Mount Stafford. It seems plausible that boromullite may have been overlooked due its similarity to sillimanite and mullite.
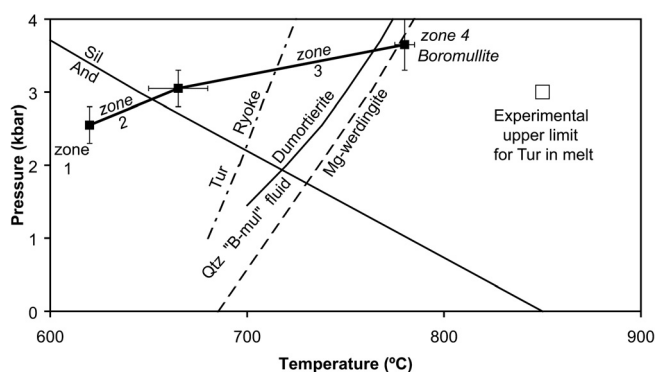

Fig. 15. Pressure-temperature diagram summarizing experimental and observational data relevant to the conditions of formation inferred for boromullite in the Mount Stafford area. Heavy line and filled squares with error bars represent the range of estimated $P - T$ conditions (White *et al.*, 2003) for the boundaries between the four metamorphic zones mapped at Mount Stafford (Fig. 9). Unfilled square: maximum temperature for tourmaline in fluid-absent partial melting experiments on a tourmaline-rich metapelite from lower-grade part of zone 2 at Mt. Stafford (Fig. 9); under these conditions tourmaline coexisted with glass (melt) (Spicer *et al.*, 2004). Sources of other data: andalusite-sillimanite relations (solid line, Pattison, 1992), dumortierite breakdown to quartz (Qtz) + "boron-mullite" ("B-Mul") + fluid in the B_2O_3-Al_2O_3-SiO_2-H_2O system (solid line, Werding & Schreyer, 1996); minimum-temperature stability of Mg-werdingite in the MgO-B_2O_3-Al_2O_3-SiO_2-H_2O system (dashed line, Werding & Schreyer, 1992); upper stability limit of schorl-dravite tourmaline (Tur) in B-poor metamorphic rocks (4–120 ppm B) as suggested for the Ryoke belt, Japan (dot-dashed line, Kawakami, 2001, 2004; Kawakami & Ikeda, 2003).

However, other considerations lead to the conclusion that boromullite may not be a common mineral. There are no assemblages incompatible with boromullite + quartz, but boromullite + quartz + cordierite is incompatible with werdingite + Al_2SiO_5, a join characteristic of most werdingite assemblages (Grew *et al.*, 1997, 1998b). Thus, it appears unlikely that boromullite would be found with both cordierite and quartz. Our proposed model for boromullite formation at Mount Stafford requires considerable melt extraction at relatively high temperature and low water activity from rocks relatively rich in boron, at least prior to melt extraction. Removal of melt depleted the rocks in both SiO_2 and B_2O_3, leaving a silica-undersaturated restite with less B_2O_3, but still enough for at least one borosilicate to appear, including boromullite if the SiO_2 content is sufficiently low. These conditions may not have been reached in many metamorphic complexes.

Instead of medium-grained prisms as in the type specimen, boromullite might be more widespread in ultrafine intergrowths such as the patches enclosed in sillimanite prisms (Fig. 12). We reconnoitred samples of B-bearing sillimanite associated with prismatine, grandidierite, boralsilite or werdingite from the Reynolds Range, central Australia, the Limpopo Belt, South Africa, Rogaland, Norway, Cap Andrahomana, Madagascar, Urungwe district, Zambia and Bok se Puts, South Africa, but did not succeed in finding any such intergrowths.

A third possibility is that boromullite could be present only in the form of Al_5BO_9 modules in B-bearing sillimanite and not as a discrete phase. Although most B-bearing sillimanite contains MgO inferred to be present in werdingite-like domains in sillimanite at the unit-cell scale, Niven *et al.* (1991) noted that achieving local charge balance on the boundaries of the werdingite-like domains required further substitutions, such as $AlSi_{-1}O_{-0.5}$ (mullite). This substitution would explain why Si decreases more than B increases, *i.e.*, $BSi_{-1.28}$ instead BSi_{-1} in B-bearing sillimanite (Grew, 1996). This B-Si relationship could also be due to the substitution $B_2MgSi_{-2}Al_{-1}O_{-1.5}$ operating in tandem with $BAlSi_{-2}O_{-1}$, the substitution due to B incorporation as Al_5BO_9 modules. Thus, B could be incorporated in sillimanite not only in werdingite-like domains, but also, to a subordinate extent, as Al_5BO_9 modules.

Dedication

This paper is dedicated to the memory of Werner Schreyer, who collaborated with Ed Grew for some 20 years on the light elements Be and B, beginning with Grew's being a Humboldt Fellow under Werner's mentorship at the Ruhr-Universität Bochum from 1983 to 1985. Werner, his colleague Günter Werding and their students were the world leaders on experiments with B-bearing systems that modelled geological systems, and thus we deemed it particularly appropriate to report a possible natural analogue of a "boron-mullite" in a special issue honouring Werner.

References

Agrell, S.O. & Smith, J.V. (1960): Cell dimensions, solid solution, polymorphism, and identification of mullite and sillimanite. *J. Amer. Ceram. Soc.*, **43**, 69-76.

Angel, R.J., McMullen, R.K., Prewitt, C.T. (1991): Substructure and superstructure of mullite by neutron diffraction. *Am. Mineral.*, **76**, 332-342.

Aramaki, S. & Roy, R. (1963): A new polymorph of Al_2SiO_5 and further studies in the system Al_2O_3-SiO_2-H_2O. *Am. Mineral.*, **48**, 1322-1347.

Balzar, D. & Ledbetter, H. (1993): Crystal structure and compressibility of 3:2 mullite. *Am. Mineral.*, **78**, 1192-1196.

Bish, D.L. & Burnham, C.W. (1992): Rietveld refinement of the crystal structure of fibrolitic sillimanite using neutron powder diffraction data. *Am. Mineral.*, **77**, 374-379.

Bloss, F.D., Gunter, M., Su, S.-C., Wolfe, H.E. (1983): Gladstone – Dale constants: A new approach. *Can. Mineral.*, **21**, 93-99.

Bowen, N.L., Greig, J.W., Zies, E.G. (1924) Mullite, a silicate of alumina. *J. Washington Acad. Sci.*, **14**, 183-191.

Bruker (1997): SHELXTL, Version 5.1. Bruker AXS Inc., Madison, Wisconsin, USA.

— (1999): SAINT+, Version 6.02. Bruker AXS Inc., Madison, Wisconsin, USA.

Buick, I.S., Stevens, G., Hermann, J., Spicer, E. (2006): The behaviour of boron during LP/HT metamorphism of metapelites, Mt. Stafford, central Australia. *Geochim. Cosmochim. Acta*, **70**, Issue 18 Supplement, A73 [abstract].

Buick, I.S., Grew, E.S., Hermann, J., Yates, M.G., Stevens, G. (2007a): Tourmaline, grandidierite-ominelite, werdingite and "boron-mullite" in boron-rich granulite-facies metapelites from Mount Stafford, central Australia. Frontiers in Mineral Sciences 2007, Programme and Abstracts, p. 272. The Mineralogical Society of Great Britain & Ireland.

Buick, I., Grew, E.S., Yates, M.G., Medenbach, O., Bebout, G.E., Clarke, G.L. (2007b): A natural analog of "boron-mullite" in granulite-facies metapelites from Mount Stafford, central Australia. *Geochim. Cosmochim. Acta*, **71**, issue 15, supplement 1, A130 [abstract].

Chorlton, L.B. (1973): The effect of boron on phase relations in the granite-water system. M.S. Thesis, McGill University, Montreal, Canada, 95 p.

Chorlton, L.B. & Martin, R.F. (1978): The effect of boron on the granite solidus. *Can. Mineral.*, **16**, 239-244.

Clarke, G.L., Collins, W.J., Vernon, R.H. (1990): Successive overprinting granulite facies metamorphic events in the Anmatjira Range, central Australia. *J. Metamorphic Geol.*, **8**, 65-88.

Collins, W.J. & Vernon, R.H. (1991): Orogeny associated with anticlockwise $P-T-t$ paths: Evidence from low-P, high-T metamorphic terranes in the Arunta inlier, central Australia. *Geology*, **19**, 835-838.

Deer, W.A., Howie, R.A., Zussman, J. (1982): Rock-forming minerals, volume 1A, Orthosilicates, 2nd edition. Longman, London, 919 p.

Dietzel, A. & Scholze, H. (1955): Untersuchungen im System B_2O_3-Al_2O_3-SiO_2. *Glastechn. Ber.*, **28**, 47-51.

Dyar, M.D., Wiedenbeck, M., Robertson, D., Cross, L.R., Delaney, J.S., Ferguson, K., Francis, C.A., Grew, E.S., Guidotti, C.V., Hervig, R.L., Hughes, J.M., Husler, J., Leeman, W., McGuire, A.V., Rhede, D., Rothe, H., Paul, R.L., Richards, I., Yates, M. (2001): Reference minerals for the microanalysis of light elements. *Geostandards Newsletter*, **25**, 441-463.

Fischer, R.X. & Schneider, H. (2008): Crystal chemistry of borates and botosilicates with mullite-type structures. *Eur. J. Mineral.*, this issue

Fischer, R.X., Schneider, H., Schmücker, M. (1994): Crystal structure of Al-rich mullite. *Am. Mineral.*, **79**, 983-990.

Garsche, M., Tillmanns, E., Almen, H., Schneider, H., Kupčik, V. (1991): Incorporation of chromium into aluminium borate $9Al_2O_3 \cdot 2B_2O_3$ (A_9B_2). *Eur. J. Mineral.*, **3**, 793-808.

Gelsdorf, G., Müller-Hesse, H., Schwiete, H.-E. (1958): Einlagerungsversuche an synthetischem Mullit und Substitutionsversuche mit Galliumoxyd und Germaniumdioxyd. Teil II. *Archiv für das Eisenhüttenwesen*, **29**(8), 513-519.

Greenfield, J.E., Clarke, G.L., White, R.W. (1998): A sequence of partial melting reactions at Mt Stafford, central Australia. *J. Metamorphic Geol.*, **16**, 363-378.

Grew, E.S. (1996): Borosilicates (exclusive of tourmaline) and boron in rock-forming minerals in metamorphic environments. *in* "Boron: Mineralogy, Petrology, and Geochemistry", E.S. Grew & L.M. Anovitz, eds., *Rev. Mineral.*, **33**, Mineralogical Society of America, Chantilly, Va., 387-502.

Grew, E.S., Yates, M.G., Shearer, C.K., Wiedenbeck, M. (1997): Werdingite from the Urungwe District, Zimbabwe. *Mineral. Mag.*, **61**, 713-718.

Grew, E.S., McGee, J.J., Yates, M. G., Peacor, D.R., Rouse, R.C, Huijsmans, J.P.P., Shearer, C.K., Wiedenbeck, M., Thost, D. E., Su, S.-C. (1998a): Boralsilite ($Al_{16}B_6Si_2O_{37}$): A new mineral related to sillimanite from pegmatites in granulite-facies rocks. *Am. Mineral.*, **83**, 638-651.

Grew, E.S., Yates, M. G., Huijsmans, J.P.P., McGee, J.J., Shearer, C.K., Wiedenbeck, M., Rouse, R.C. (1998b) Werdingite, a borosilicate new to granitic pegmatites. *Can. Mineral.*, **36**, 399-414.

Grew, E.S., Graetsch, H., Pöter, B., Yates, M.G., Buick, I., Bernhardt, H.-J., Schreyer, W, Werding, G., Carson, C.J., Clarke, G.L. (2008): Boralsilite, $Al_{16}B_6Si_2O_{37}$, and "boron-mullite": compositional variations and associated phases in experiment and nature. *Am. Mineral.*, **93**, 282-299.

Griesser, K.J., Beran, A., Voll, D., Schneider, H. (2008) Boron incorporation into mullite. Mineral. and Petrol., **92**, 309-320.

Ihara, M., Imai, K., Fukunaga, J., Yoshida, N. (1980): Crystal structure of boroaluminate, $9Al_2O_3 \cdot 2B_2O_3$. Yogyo-Kyokai-Shi **88**(2), 77-84 [in Japanese with English abstract].

Kawakami, T. (2001): Boron depletion controlled by the breakdown of tourmaline in the migmatite zone of the Aoyama area, Ryoke metamorphic belt, southwestern Japan. *Can. Mineral.*, **39**, 1529-1546.

Kawakami, T. (2004): Tourmaline and boron as indicators of the presence, segregation and extraction of melt in pelitic migmatites: examples from the Ryoke metamorphic belt, SW Japan. *Trans. Royal Soc. Edinburgh: Earth Sci.*, **95**, 111-123.

Kawakami, T. & Ikeda, T. (2003): Boron in metapelites controlled by the breakdown of tourmaline and retrograde formation of borosilicates in the Yanai area, Ryoke metamorphic belt, SW Japan. *Contrib. Mineral. Petrol.*, **145**, 131-150.

Letort, Y. (1952): Contribution à l'étude de la synthèse de la mullite. *Trans. Internat. Ceramic Congress*, 19-32.

Mandarino, J.A. (1981): The Gladstone – Dale relationship: Part IV. The compatibility concept and its application. *Can. Mineral.*, **19**, 441-450.

McGee, J.J. & Anovitz, L.M. (1996): Electron probe microanalysis of geologic materials for boron. *in* "Boron: Mineralogy, Petrology, and Geochemistry", E.S. Grew & L.M. Anovitz eds., *Rev. Mineral.*, **33**, Mineralogical Society of America, Chantilly, Va., 771-788.

Medenbach, O. (1985): A new microrefractometer spindle-stage and its application. *Fortschr. Mineral.*, **63**, 111-133.

— (1986): Ein modifiziertes Kristallbohrgerät nach Verschure (1978) zur Isolierung kleiner Einkristalle aus Dünnschliffen. *Fortschr. Mineral*, Beiheft **64**(1), 113 [abstract].

Merlet, C. (1994): An accurate computer correction program for quantitative electron-probe microanalysis. *Mikrochim. Acta*, **114**, 363-376.

Moore, J.M., Waters, D.J., Niven, M.L. (1990): Werdingite, a new borosilicate mineral from the granulite facies of the western Namaqualand metamorphic complex, South Africa. *Am. Mineral.*, **75**, 415-420

Niven, M.L., Waters, D.J., Moore, J.M. (1991): The crystal structure of werdingite, $(Mg,Fe)_2Al_{12}(Al,Fe)_2Si_4(B,Al)_4O_{37}$, and its relationship to sillimanite, mullite, and grandidierite. *Am. Mineral.*, **76**, 246-256.

Patiño Douce, A.E. (1993): Titanium substitution in biotite: an empirical model with applications to thermometry, O_2 and H_2O barometries, and consequences for biotite stability. *Chem. Geol.*, **108**, 133-162.

Pattison, D.R.M. (1992): Stability of andalusite and sillimanite and the Al_2SiO_5 triple point: Constraints from the Ballachulish aureole, Scotland. *J. Geol.*, **100**, 423-446.

Rubatto, D., Hermann, J., Buick, I.S. (2006): Temperature and bulk composition control on the growth of monazite and zircon during low-pressure anatexis (Mount Stafford, central Australia). *J. Petrol.*, **47**, 1973-1996.

Scholze, H. (1956): Über Aluminiumborate. *Z. anorg. allgemeine Chem.*, **284**, 272-277.

Shape Software (2006): Crystal structure drawing program ATOMS V6.3.1.

Sokolova, Ye.V., Azizov, A.V., Simonov, M.A., Leonyuk, N.I., Belov, N.V. (1978): Crystal structure of synthetic ortho-3-borate $Al_5(BO_3)O_6$. *Doklady Akad. Nauk SSSR*, **243**, 655-658 [in Russian].

Spicer, E.M., Stevens, G., and Buick, I.S. (2004): The low-pressure partial-melting behaviour of natural boron-bearing metapelites from the Mt. Stafford area, central Australia. *Contrib. Mineral. Petrol.*, **148**, 160-179.

Vernon, R.H., Clarke, G.L., Collins, W.J. (1990): Local, mid-crustal granulite facies metamorphism and melting: an example in the Mount Stafford area, central Australia. *in* "High-temperature metamorphism and crustal anatexis", J.R. Ashworth & M. Brown, eds. *The Mineralogical Society Series*, **2**, 272-319.

Werding, G. & Schreyer, W. (1984): Alkali-free tourmaline in the system $MgO-Al_2O_3-B_2O_3-SiO_2-H_2O$. *Geochim. Cosmochim. Acta*, **48**, 1331-1344.

—, — (1992): Synthesis and stability of werdingite, a new phase in the system $MgO – Al_2O_3 – B_2O_3 – SiO_2$ (MABS), and another new phase in the ABS-system. *Eur. J. Mineral.*, **4**, 193-207

—, — (1996): Experimental studies on borosilicates and selected borates. *in* "Boron: Mineralogy, Petrology, and Geochemistry", E.S. Grew & L.M. Anovitz, eds., *Rev. Mineral.*, **33**, Mineralogical Society of America, Chantilly, Va., 117-163.

White, R.W., Powell, R., Clarke, G.L. (2003): Prograde metamorphic assemblage evolution during partial melting of metasedimentary rocks at low pressures: migmatites from Mt Stafford, central Australia. *J. Petrol.*, **44**, 1937-1960.

Yvon, K., Jeitschko, W., Parthe, E. (1977): LAZY PULVERIX, a computer-program, for calculating X-ray and neutron-diffraction powder patterns. *J. Appl. Crystallogr.*, **10**, 73-74.